*Physics and Simulation of Optoelectronic Devices VIII, ed. R. Binder, P. Blood & M. Osinski, SPIE Proc. 3944, 2000.*

# Simulation and Optimization of 420 nm InGaN/GaN Laser Diodes

Joachim Piprek[*] [a], R. Kehl Sink [a], Monica A. Hansen [b], John E. Bowers [a], and Steve P. DenBaars [b]

[a] Electrical and Computer Engineering Department
[b] Materials Department
University of California at Santa Barbara, Santa Barbara, CA 93106

## ABSTRACT

Using self-consistent laser simulation, we analyze the performance of nitride Fabry-Perot laser diodes grown on sapphire. The active region contains three 4 nm InGaN quantum wells. It is sandwiched between GaN separate confinement layers and superlattice AlGaN/GaN cladding layers. AlGaN is used as an electron barrier layer. Pulsed lasing is measured near 420 nm wavelength and at temperatures up to 120°C. Advanced laser simulation is applied to link microscopic device physics to measurable device performance. Our two-dimensional laser model considers carrier drift and diffusion including thermionic emission at hetero-boundaries. The local optical gain is calculated from the wurtzite band structure employing a non-Lorentzian line broadening model. All material parameters used in the model are evaluated based on recent literature values as well as our own experimental data. Simulation results are in good agreement with measurements. Multi-lateral mode lasing is calculated with a high order vertical mode. The carrier distribution among quantum wells is found to be strongly non-uniform leading to a parasitic (absorbing) quantum well. The influence of defect recombination, vertical carrier leakage and lateral current spreading is investigated. The reduction of such carrier losses is important to achieve lower threshold currents and less self-heating. Several device optimization options are proposed. Elimination of the parasitic quantum well is shown to substantially enhance the device performance.

**Keywords:** InGaN, blue laser diode, nitride semiconductor laser, quantum well devices, numerical analysis, semiconductor device modeling

## 1. INTRODUCTION

Violet InGaN/GaN laser diodes have been pioneered by Nakamura et al.[1] and are now commercially available.[2] These laser diodes have potential in a number of applications such as optical storage, printing, full-color displays, chemical sensors and medical applications. The data capacity of digital versatile disks (DVDs) can be increased from 4.7 to more than 15 gigabites by using InGaN lasers instead of red AlInGaP lasers.[1] The estimated InGaN laser lifetime under room-temperature (RT) continuous-wave (CW) operation has been improved to more than 10,000 hours by using laterally epitaxially overgrown GaN as substrate and AlGaN/GaN strained-layer superlattices (SLS) as cladding layers.[3] Threshold current densities as low as 1.2 kA/cm$^2$ were achieved using $In_{0.15}Ga_{0.85}N$ quantum wells (QWs).[4] Fundamental transverse mode operation up to 30 mW output power and with a slope efficiency as high as 1 W/A was obtained using a ridge-waveguide laser with 2 μm ridge width.[5] These lasers have cleaved facets with one facet coated by two pairs of quarter-wave $TiO_2/SiO_2$ dielectric multilayers.

Since the first announcement of a nitride laser diode by Nakamura et al. in December 1995, more than 10 other research groups have succeeded in fabricating similar laser diodes. However, only about half of these groups have achieved RT-CW lasing so far.[6] In 1997, researchers of our university demonstrated an InGaN laser diode employing uncoated reactive ion etched (RIE) facets.[7] The structural properties of RIE facets are far from ideal leading to poor optical feedback. Despite several design improvements during the last two years, RT-CW operation has not yet been achieved with these RIE lasers.[8] Major technological challenges remain as well as the need for a more detailed understanding of nitride laser physics. Advanced numerical laser simulation can help to establish quantitative links between microscopic material properties and measured device performance.

[*] Correspondence: Email: piprek@ece.ucsb.edu, WWW: http://eci.ucsb.edu/~piprek, Telephone: 805-893-4051

In this paper, we present first results of a self-consistent numerical simulation of our InGaN laser diodes. We use a commercial laser diode software package[9] that combines band structure and gain calculations with two-dimensional (2D) simulations of wave guiding, current flow, and heat flux. The model considers carrier drift and diffusion including thermionic emission at hetero-boundaries. This allows for a study of vertical carrier leakage, lateral current spreading, and defect recombination. The reduction of such carrier losses is important to achieve lower threshold currents and less self-heating. The local optical gain is calculated from the wurtzite band structure including valence mixing and strain effects. A non-Lorentzian line broadening model is utilized and many-body effects are considered. Transversal multimode lasing is taken into account including higher order vertical modes. Such a comprehensive model requires more than 40 material parameters per epitaxial layer, most of which are not exactly known. We carefully evaluated all material parameters based on recent literature values as well as our own experimental data. However, material parameters remain the main source of uncertainty in our model.

Section 2 gives a brief description of device structure and experimental results. Section 3 provides details of the theoretical model and of material parameters used. Section 4 presents a microscopic analysis of laser physics based on simulation results. Section 5 discusses device optimization options.

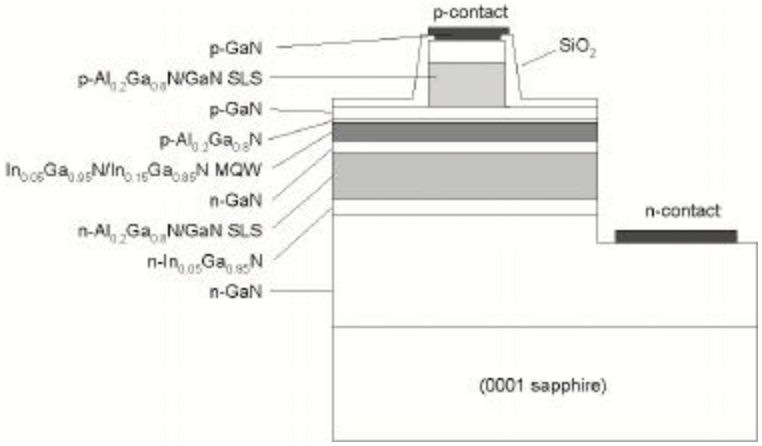


Fig. 1: Schematic cross section of our laser diodes.

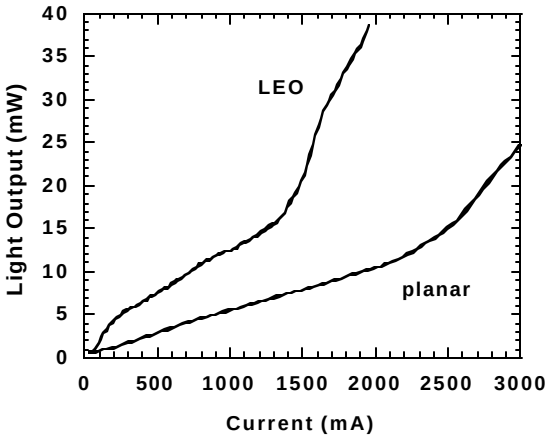


Fig. 2: Measured light vs. current characteristics.

## 2. DEVICE STRUCTURE AND EXPERIMENTAL RESULTS

The schematic structure of our InGaN multiple-quantum-well (MQW) laser diodes is given in Fig. 1. The laser is grown on a lateral epitaxial overgrowth (LEO) GaN substrate to reduce the dislocation density. Details of growth and processing are described elsewhere.[10] Table 1 lists compositions, layer thicknesses, and doping densities. To achieve sufficient waveguiding, the $Al_{0.09}Ga_{0.91}N$ cladding regions need to be relatively thick and they are grown as $Al_{0.18}Ga_{0.82}N$/GaN superlattices. Laser facets are formed by $Cl_2$ reactive ion etching (RIE) of 45 μm wide mesas of various lengths ranging from L = 400 μm to 1600 μm. Contact stripes are patterned on these mesas with widths ranging from W = 5 μm to 15 μm. The structure was etched around the p-contact stripe through the p-cladding for index guiding. The n- and p-contacts are formed by electron beam evaporation of Ti/Al and Pd/Au, respectively. Electrical testing was performed using 50 ns pulses with a 1 kHz pulse repetition rate. Figure 2 shows the typical pulsed light output per uncoated facet of a laser diode grown on LEO GaN and a laser diode grown on planar GaN as a function of forward current. Due to a reduction in nonradiative recombination, the minimum threshold current density $j_{th}$ is reduced from 10 kA/cm$^2$ for laser diodes grown on planar GaN to 4.8 kA/cm$^2$ for laser diodes grown on LEO GaN. The latter exhibit an improved slope efficiency $\eta_d$ up to 3.2 % per facet. However, there are large variations among devices and typical numbers for LEO GaN lasers as shown in Fig. 2 are $j_{th}$ = 12 kA/cm$^2$ and $\eta_d$ = 0.04 W/A = 1.3% (W=5 μm, L=1600 μm). The measured slope efficiency does not represent the entire light

emitted on each side. About 60 % of the light power is not detected, which is attributed to photon scattering at the rough RIE facet, to its tilted angle, and to laser beam interference with the remaining GaN substrate.[11] The facet reflectance is estimated to be only R = 0.05, considerably less than the ideal value of 0.18.[12] Considering these numbers, the inverse slope efficiency vs. cavity length plot gives $\eta_i$ = 22 % internal efficiency and $\alpha_i$ = 42 $cm^{-1}$ internal optical loss for our LEO GaN lasers.[10]

| LAYER | MATERIAL | THICKNESS [nm] | DOPING [$10^{18}cm^{-3}$] |
|---|---|---|---|
| contact | GaN | 100 | 75 (Mg) |
| cladding | $Al_{0.18}Ga_{0.82}N$/GaN SL | 451 | 75 (Mg) |
| waveguide | GaN | 90 | 75 (Mg) |
| electron stopper | $Al_{0.2}Ga_{0.8}N$ | 20 | 100 (Mg) |
| waveguide | GaN | 8.5 | 0.05 (Si) |
| barrier | $In_{0.04}Ga_{0.96}N$ | 8.5 | 0.05 (Si) |
| quantum well | $In_{0.13}Ga_{0.87}N$ | 4.0 | 0.05 (Si) |
| barrier | $In_{0.04}Ga_{0.96}N$ | 8.5 | 6.5 (Si) |
| quantum well | $In_{0.13}Ga_{0.87}N$ | 4.0 | 0.05 (Si) |
| barrier | $In_{0.04}Ga_{0.96}N$ | 8.5 | 6.5 (Si) |
| quantum well | $In_{0.13}Ga_{0.87}N$ | 4.0 | 0.05 (Si) |
| barrier | $In_{0.04}Ga_{0.96}N$ | 8.5 | 6.5 (Si) |
| waveguide | GaN | 98.5 | 6.5 (Si) |
| cladding | $Al_{0.18}Ga_{0.82}N$/GaN SL | 451 | 2.0 (Si) |
| compliance layer | $In_{0.05}Ga_{0.95}N$ | 100 | 6.0 (Si) |
| substrate | GaN | 2000 | 6.0 (Si) |

Table 1: Layer parameters as used in the simulation.

## 3. THEORETICAL MODEL AND MATERIAL PARAMETERS

LASTIP self-consistently combines 2D carrier transport, heat flux, optical gain computation, and wave guiding within the transversal plane (x,y). Longitudinal variations are of minor importance in our device. Heat flux calculations are not included in our analysis of pulsed laser operation. Further details of the laser model are published elsewhere.[13] We discuss here only those aspects that are crucial to our analysis.

The drift-diffusion model of carrier transport includes Fermi statistics and thermionic emission at hetero-barriers. Thermionic emission is mainly controlled by the offset of conduction band ($\Delta E_c$) and valence band ($\Delta E_v$) at hetero-barriers. For AlGaN/GaN and InGaN/GaN we use a band offset ratio ($\Delta E_c/\Delta E_v$) of 0.67/0.33 [14] and 0.3/0.7,[15] respectively. Due to the small conduction band offset in the InGaN MQW, vertical electron leakage into the p-side GaN waveguide layer is a crucial issue with nitride lasers, requiring an AlGaN barrier layer above the MQW (cf. Fig. 1). The room temperature band gap $E_g$ of our ternary alloys is calculated from [14, 16]

$$E_g\,(Al_xGa_{1-x}N)\,[eV] = 6.28\,x + 3.42\,(1-x) - 0.98\,x\,(1-x) \quad (1)$$

$$E_g\,(In_xGa_{1-x}N)\,[eV] = 1.89\,x + 3.42\,(1-x) - 3.8\,x\,(1-x) \quad (2)$$

A major handicap with nitride semiconductors is the high activation energy of the Mg acceptor which causes the hole density to be considerably smaller than the Mg density. We use an Mg activation energy of 170 meV for GaN [17] which is assumed to increase by 3meV per % Al for AlGaN.[6] A uniform hole mobility of 2 $cm^2/Vs$ is assumed [18] which is only a

rough estimate, in particular for the p-side AlGaN/GaN superlattice. In n-type material, the Si donor activation energy is about 20 meV.[19] Our electron mobility values are 200 $cm^2/Vs$ for GaN, 100 $cm^2/Vs$ for InGaN, and 30 $cm^2/Vs$ for AlGaN.[18] Within passive layers, a spontaneous emission parameter of $B = 2 \times 10^{-10}\ cm^3 s^{-1}$ is employed.[20] The spontaneous recombination rate in quantum wells is much larger than in passive layers and it is calculated self-consistently by integration of the spontaneous emission spectrum. The Shockley-Read-Hall (SRH) recombination lifetime of electrons and holes is assumed to be 1 ns, however, this is only a rough estimate since type and density of recombination centers are very much technology dependent. The GaN Auger parameter $C = 2 \times 10^{-31}\ cm^6/s$ is relatively small,[21] nevertheless, Auger recombination might become important at high carrier densities.

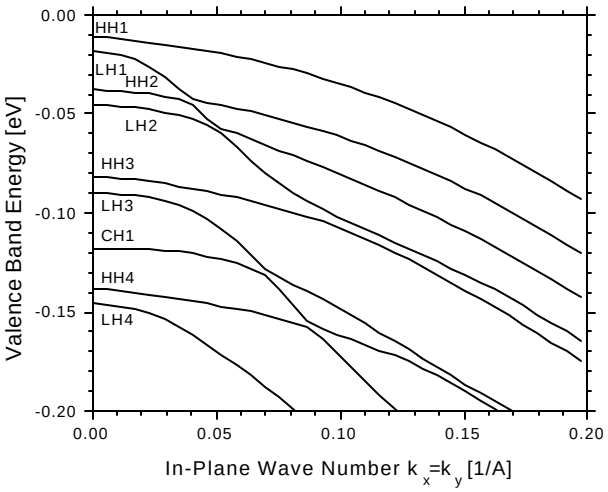


Fig. 3: In-plane dispersion of valence subbands.

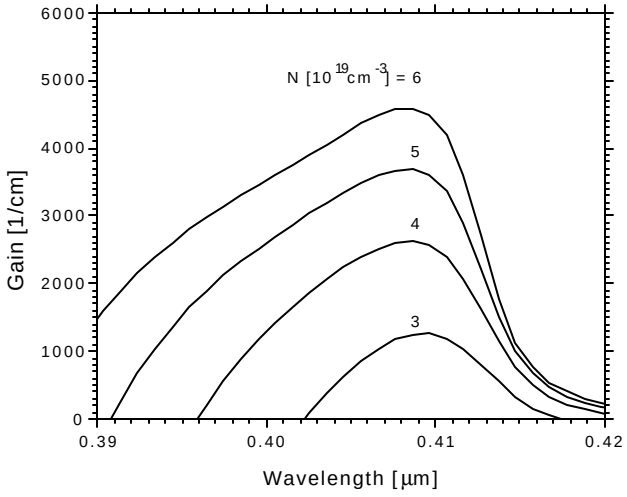


Fig. 4: Gain spectra for different carrier densities N.

In our strained $In_{0.13}Ga_{0.87}N/In_{0.04}Ga_{0.96}N$ quantum wells, the conduction bands are assumed to be parabolic and the non-parabolic valence bands are computed by the **kp** method including valence band mixing.[22] Valence band effective mass parameters ($A_1$ - $A_6$) are obtained from Ref.[23] , GaN values are used for the crystal field split energy $\Delta_1 = 16$ meV and for the spin-orbit split energies $\Delta_2 = \Delta_3 = 4$ meV as well as for the deformation potentials.[22] Elastic constants are linearly interpolated between $C_{13} = 114$ GPa and $C_{33} = 381$ GPa given for GaN and $C_{13} = 94$ GPa and $C_{33} = 200$ GPa given for InN.[24] Vegard's law is applied to obtain the ternary lattice constant from a = 0.3548 nm (InN), 0.3189 nm (GaN), and 0.3112 nm (AlN).[25] These parameters give 1.4 % compressive biaxial strain in our quantum wells and 0.4 % in the barriers. The calculated heavy-hole (HH), light-hole (LH) and crystal-field split-hole (CH) bands are shown in Fig. 3, illustrating the strong valence band mixing. Similar band structures of InGaN quantum wells have been calculated by Yeo et al.[26] For structures like ours, grown along the c-axis, the quantum well strain is biaxial, lowering the CH band but hardly separating HH and LH bands, i.e., strain is not as effective in reducing the threshold carrier density as in GaAs or InP based lasers. Uniaxial strain promises lower threshold currents.[27]

For gain computation, a non-Lorentzian line broadening model is utilized following Asada [28] and using a longitudinal optical phonon energy of 90 meV.[25] At room temperature and with $N = 10^{19}\ cm^{-3}$ carrier density, the effective intraband relaxation time becomes 15 fs which is in good agreement with other publications.[29, 30] Band gap shrinkage caused by carrier-carrier interaction is considered as $\Delta E_g = -\xi N^{1/3}$, the renormalization parameter $\xi = 4.5 \times 10^{-8}$ eVcm for our 4 nm thick quantum wells is extracted from Ref.[31] . Recently, there have been several publications on piezoelectric field effects on spontaneous and stimulated emission in InGaN quantum wells (see, e.g., Ref.[30] and Ref.[32] ). The wider the quantum well, the stronger electrons and holes are separated by the piezoelectric field, thereby reducing optical gain as well as spontaneous emission. However, screening by quantum confined carriers[30] and mainly by free carriers[33] is expected to suppress piezoelectric field effects at typical threshold carrier densities of $3 \times 10^{19}\ cm^{-3}$. The high threshold carrier density is also assumed to eliminate exciton enhancements of the gain, despite the large exciton binding energy in nitrides.[34] Considering a GaN exciton Bohr radius of $r_B = 1.6$ nm,[31] the excitonic phase becomes unstable as the 2D electron-hole density exceeds $1/\pi r_B^2 = 1.2 \times 10^{13}\ cm^{-2}$,

corresponding to N = 3 × $10^{19}$cm$^{-3}$ in our quantum wells. Structural non-uniformities within the quantum well may also affect the optical gain.[35] However, QW carrier localization does not seem to dominate the gain of nitride lasers.[1] In summary, the gain mechanism in real nitride lasers is a very complex issue and it is not yet fully understood. Comprehensive laser simulation will help to link microscopic gain mechanisms to the macroscopic device performance. Assuming uniform rectangular quantum wells, we obtain for our laser the gain spectra given in Fig. 4. The gain peak near 409 nm includes contributions from the HH1 subband as well as from the LH1 subband (cf. Fig. 3).

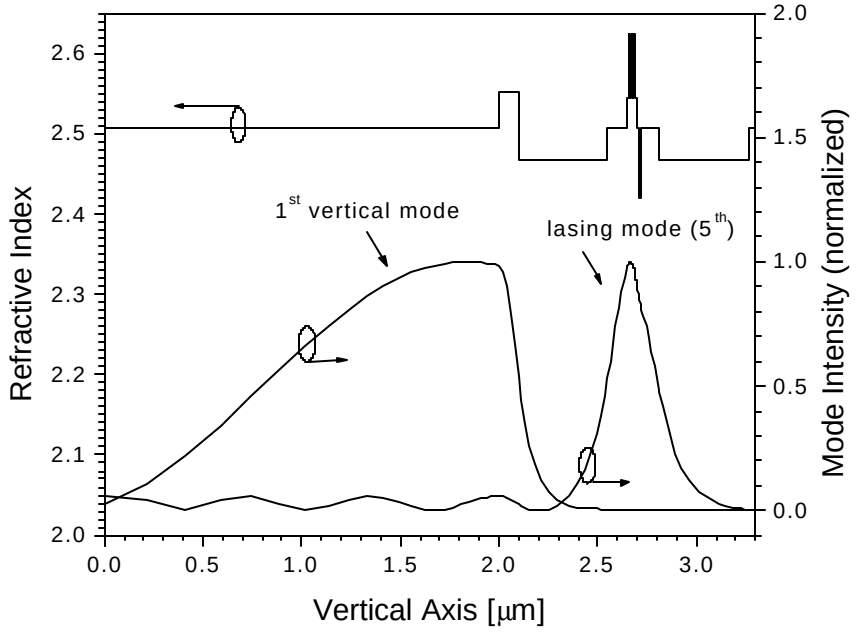


Fig. 5: Vertical profiles of refractive index and optical modes.

Our simulation of the 2D optical waveguide adopts the measured parameters for the internal loss ($\alpha_i$ = 42 cm$^{-1}$) and for the power reflectance per facet (R = 0.05) giving a distributed mirror loss coefficient of $\alpha_m$ = 19 cm$^{-1}$ for the longest cavity length (L = 1600 μm) which will be used in the following. The refractive index of ternary alloys is extracted from GaN waveguide measurements [36] using bandgap variations in the model (x<0.3) [37]

$$n\,(Al_xGa_{1-x}N) = 2.5067 - 0.43\,x \qquad (3)$$

$$n\,(In_xGa_{1-x}N) = 2.5067 + 0.91\,x \qquad (4)$$

The resulting vertical index profile is plotted in Fig. 5 (using an average index for the superlattice) together with the 1$^{st}$ order and the 5$^{th}$ order mode of the vertical waveguide. Only the 5$^{th}$ order mode has sufficient overlap with the MQW active region to contribute to lasing, all lower order vertical modes do not lase in our simulation. Lasing of high order vertical modes was observed experimentally by several groups.[38, 39] The extension of the lasing mode into the GaN substrate leads to a reduced optical confinement factor and to higher optical loss. In our lasers, the facets are not etched through the GaN substrate, i.e., the substrate part of the lasing mode does not receive feedback and leaks out. Mode leaking is hard to consider in our simulation. We assume that the corresponding optical loss is already included in the measured parameters (R, $\alpha_i$) and we neglect the substrate part of the optical mode in the following Sections. Besides the high-order vertical mode, our index guided structure also exhibits several lateral lasing modes (W = 5 μm). Figure 6 shows normalized intensity plots of the first three lateral modes (the top ridge extends from x =10 μm to x = 15 μm).

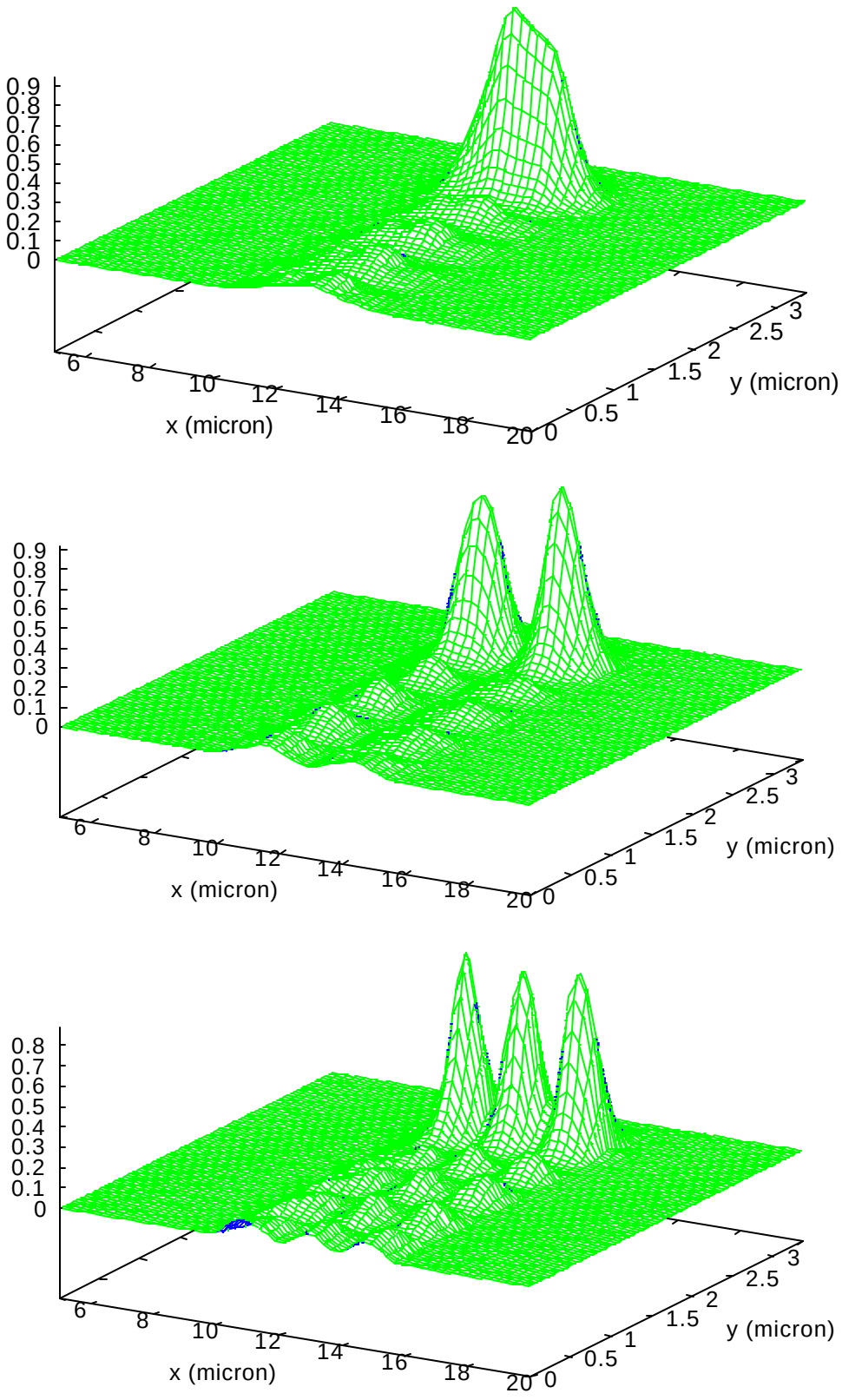


Fig. 6. First three lateral (x) lasing modes (normalized, all are 5th order vertical (y) modes).

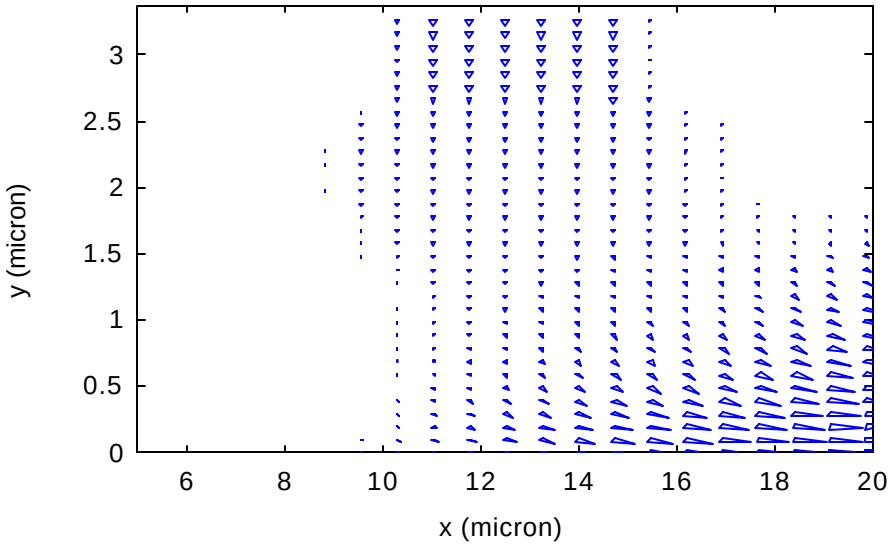


Fig. 7: 2D vector plot of the current flow (same window as in Fig. 6)

## 4. SIMULATION AND ANALYSIS

Figure 7 shows the current spreading towards the n-contact (cf. Fig. 1). Lateral spreading of holes within the top p-GaN waveguide layer and within the active region is illustrated in Fig. 8 which shows the x-component of the hole current density within the waveguide region (from n-cladding to p-cladding). The lateral hole current peaks near the edge of the ridge and the AlGaN barrier layer clearly separates the two current paths. Hole spreading within the p-GaN waveguide layer is stronger than within the quantum wells. The vertical y-component of the electron current is given in Fig. 9 within the same region. It illustrates that the electrons recombine almost completely within the MQW region underneath the ridge, i.e., the adjacent AlGaN barrier layer prevents electrons from entering the p-GaN waveguide layer. However, some electrons leak out of the p-side quantum well at the edges of the active region and recombine with holes underneath the AlGaN barrier layer.

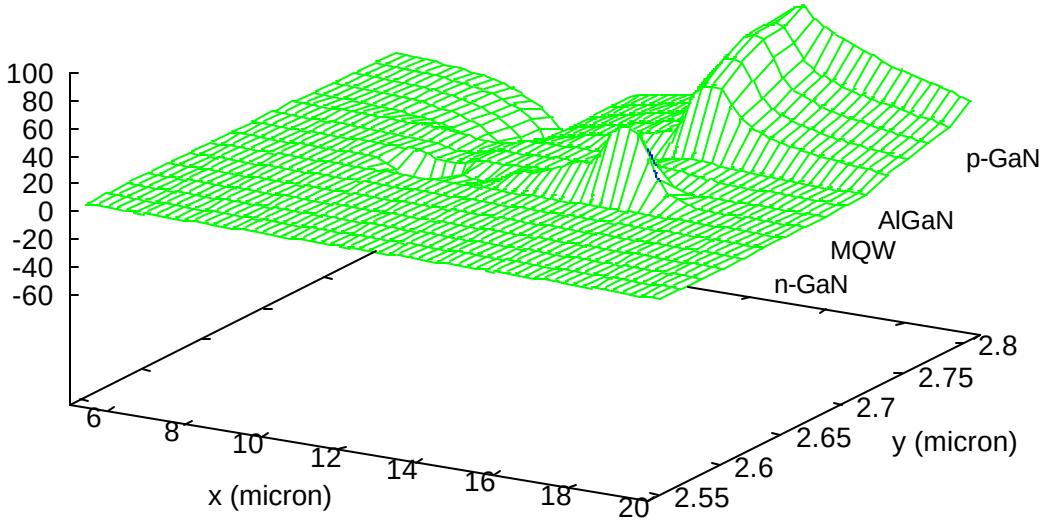


Fig. 8: Lateral hole current density $j_{p,x}(x,y)$ [A/cm$^2$] within the waveguide region.

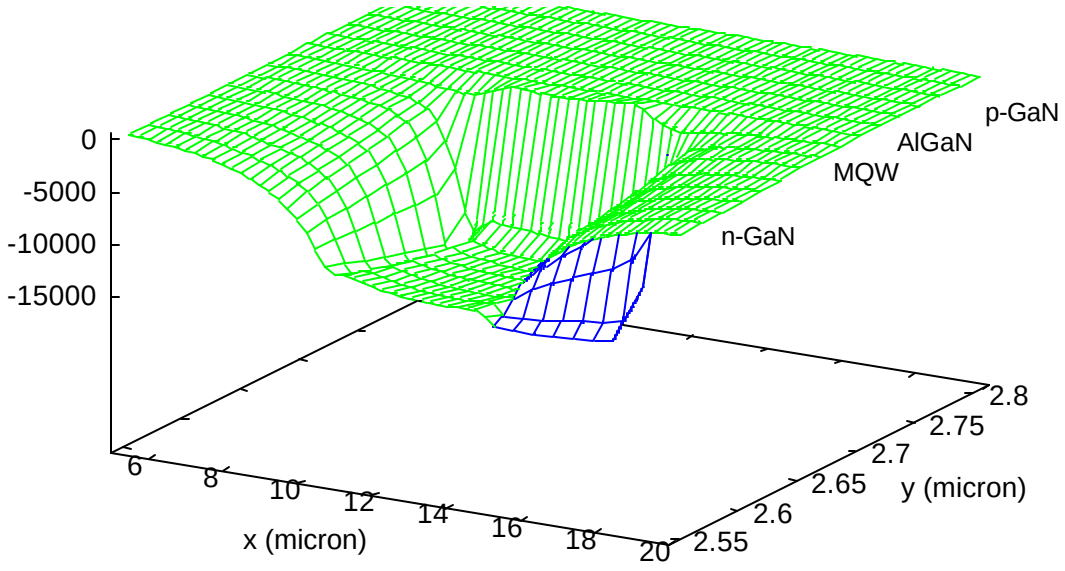


Fig. 9: Vertical electron current density $j_{n,y}(x,y)$ [A/cm$^2$] within the waveguide region.

Strong non-uniformity of the vertical carrier distribution among five quantum wells has been pointed out by Domen et al. and the use of three quantum wells instead has been proven advantageous.[40] In our case of three quantum wells we still find a significant carrier non-uniformity (Fig. 10). As a consequence, the n-side QW does not reach transparency and only the other two QWs provide gain for lasing. Removal of the parasitic quantum well will be shown to substantially enhance the laser performance (see Sect. 5). The carrier non-uniformity increases with higher current injection. This effect was recently found to strongly reduce the internal quantum efficiency of MQW lasers.[41] Figure 11 gives the energy diagram for our MQW region and the quasi Fermi levels near threshold. Within the quantum wells, the hole Fermi level is inside the first valence-subband and it touches the second subband in the p-side quantum well (cf. Fig. 3).

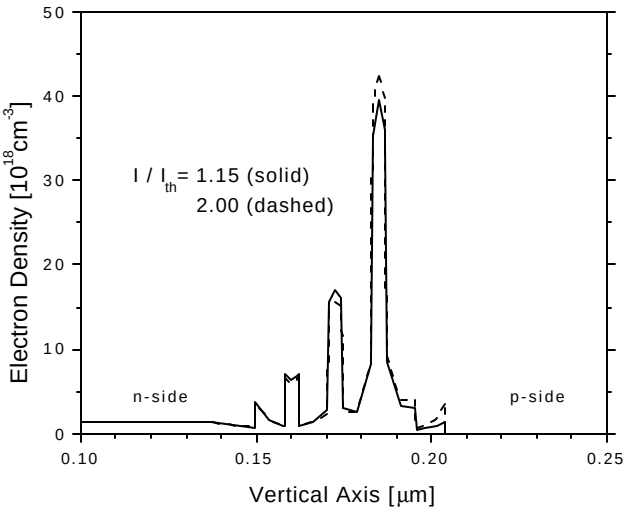


Fig. 10: Vertical electron density profile within the MQW region.

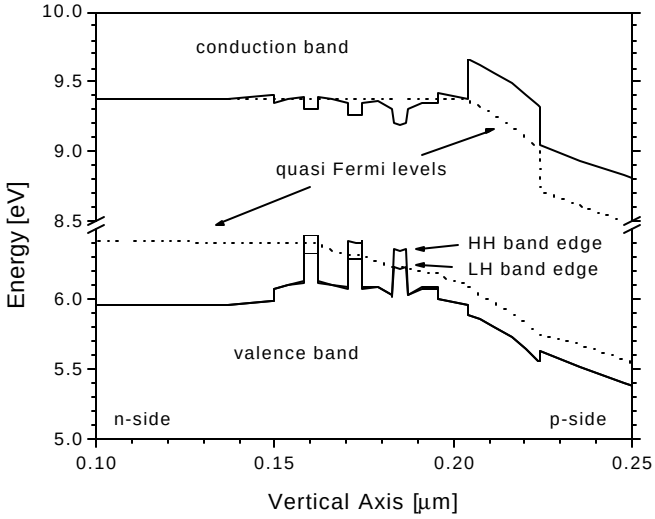


Fig. 11: Energy band diagram of the MQW region.

Calculated light vs. current (LI) characteristics are shown in Fig. 12. The threshold current is close to our typical experimental results (cf. Fig. 2). It is about twice as high as our best results. The large variation of our experimental results is mainly caused by structural differences among lasers which are hard to evaluate. However, the rate of one or several recombination mechanisms may also be too large in our simulation. The influence of defect recombination is illustrated by the dotted curve in Fig. 12 which is calculated with an overall carrier lifetime of 1 μs, effectively eliminating defect recombination from the model. Thus, about 40 % of the threshold current are caused by defect recombination. The dashed curve in Fig. 12 is calculated for a laser which is completely etched (width 5 μm, bottom n-contact) thereby eliminating any current spreading (the slight improvement of the lateral mode confinement is of minor importance). This reduces the threshold current by 32 %, i.e., almost one third of the current is normally lost in lateral leakage. The slope efficiency of our full simulation is 17 % (total power), it is affected by current spreading, and it is slightly improved with reduced defect recombination (Fig. 12). Considering 60% loss in light detection, we obtain $\eta_d$ = 3.4 % per facet which is very close to our best measured result (3.2 %). Thus, our first simulation is in surprisingly good agreement with the measurement.

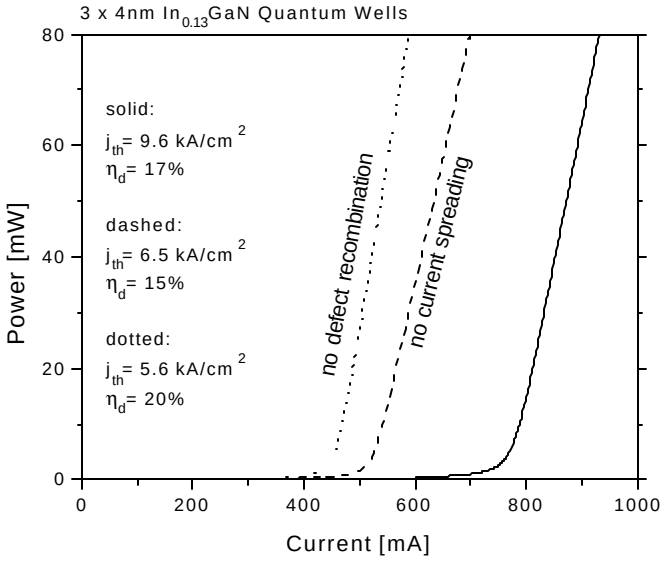


Fig. 12: Calculated LI characteristics (3 QWs).

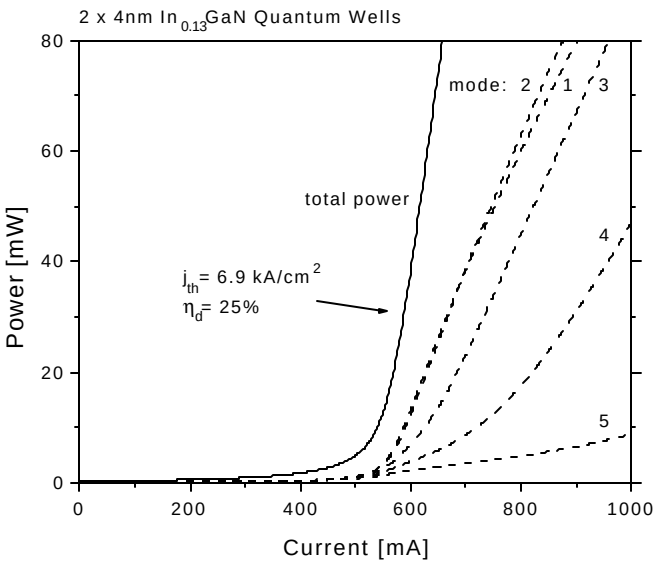


Fig. 13: LI characteristic for 2 QWs (dashed: lateral modes).

## 5. DESIGN OPTIMIZATION

Several suggestions for design optimization can be derived from these first simulations, some of which have already been demonstrated by Nakamura. First, a thicker n-AlGaN cladding layer will help to better suppress the leaky optical field in the GaN substrate.[1] However, this AlGaN/GaN superlattice has a low thermal conductivity and its increased thickness would lead to increased self-heating. Second, a smaller ridge is expected to eliminate higher order lateral modes.[5] Third, deeper etching of the p-ridge will reduce the lateral current spreading. However, etching through the MQW may lead to undesirable high surface recombination. Fourth, the use of 2 instead of 3 quantum wells promises lower threshold currents.[4] Here, we evaluate only the fourth option for our laser. Figure 13 shows that the resulting threshold current is 28% lower than before and that the slope efficiency is improved by a factor of 1.5. Figure 13 also shows the contribution of the first 5 lateral modes to the lasing power. The second mode dominates at higher current, in agreement with our results for 3 quantum wells (not shown). The main reason for the performance differences is illustrated in Fig. 14. With 3 quantum wells (dashed), the n-side well does not reach transparency (cf. Fig. 10) and it absorbs photons generated by the other two wells. This parasitic well can be eliminated by using only 2 quantum wells (solid). At the same current as before (1440mA), two quantum wells now generate more light than 3 QWs before. The threshold carrier density is smaller because of less absorption and a larger

part of the total current goes into stimulated recombination. The lateral gain profile in both quantum wells shows good carrier confinement and strong absorption outside the ridge region (Fig. 15).

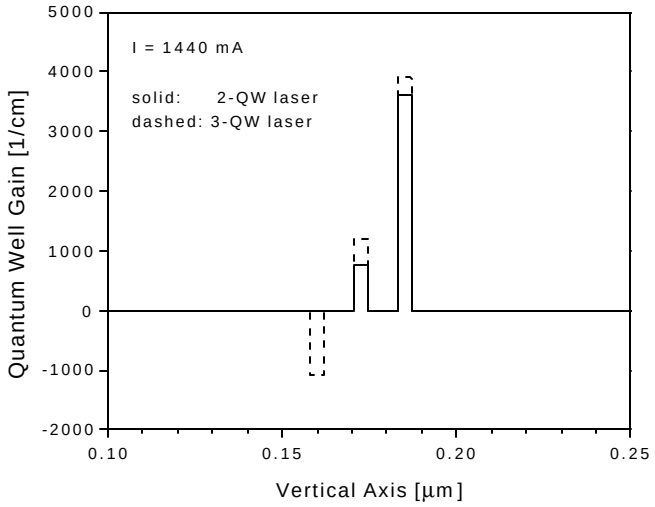


Fig. 14: Average gain per quantum well.

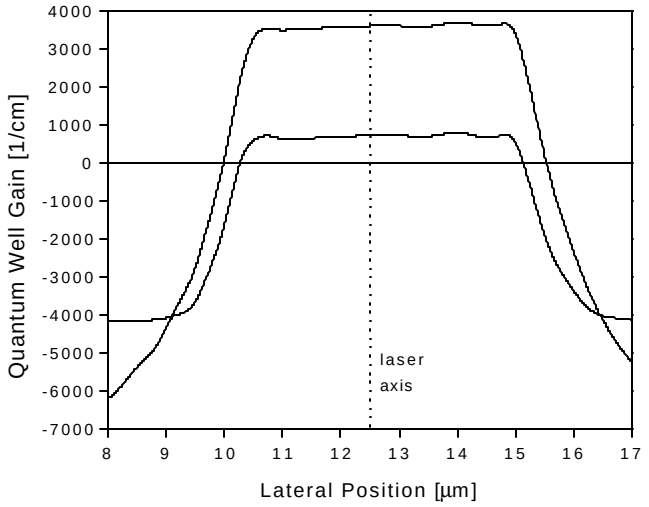


Fig. 15: Lateral profile of local gain in both quantum wells.

## 6. CONCLUSION

We have presented, to our knowledge, the currently most comprehensive simulation of a wurtzite InGaN/GaN laser diode. Careful selection of material parameters leads to a good agreement with measurements. We find that defect recombination causes about 40% of our threshold current and that one third of the current is lost by lateral leakage. Vertical electron leakage is effectively reduced by our AlGaN barrier layer. The $5^{th}$ order vertical lasing mode includes a considerable amount of optical power that leaks out through the GaN substrate. Carrier non-uniformity among the quantum wells creates a parasitic well which absorbs photons generated in the other two wells. Removal of the parasitic well is expected to reduce the threshold current by one third and to give 1.5 times higher quantum efficiency. However, more experimental and theoretical investigations are required to improve the knowledge of crucial material parameters. Our future work will also address thermal issues.

## REFERENCES


1. S. Nakamura, "InGaN-based violet laser diodes," *Semiconductor Science and Technology* **14**, pp. R27-40, 1999.
2. Nichia Corporation (http://www.mesh.ne.jp/nichia/), 1999.
3. S. Nakamura, M. Senoh, S. I. Nagahama, N. Iwasa, T. Yamada, T. Matsushita, H. Kiyoku, Y. Sugimoto, T. Kozaki, H. Umemoto, M. Sano, and K. Chocho, "InGaN/GaN/AlGaN-based laser diodes with modulation-doped strained-layer superlattices," *Japanese Journal of Applied Physics, Part 2 (Letters)* **36**, pp. 1568-71, 1997.
4. S. Nakamura, M. Senoh, S. I. Nagahama, N. Iwasa, T. Yamada, T. Matsushita, H. Kiyoku, Y. Sugimoto, T. Kozaki, I. Umemoto, M. Sano, and K. Chocho, "InGaN/GaN/AlGaN-based laser diodes grown on GaN substrates with a fundamental transverse mode," *Japanese Journal of Applied Physics, Part 2 (Letters)* **37**, pp. L1020-2, 1998.

5. S. Nakamura, M. Senoh, S. I. Nagahama, T. Matsushita, K. Kiyoku, Y. Sugimoto, T. Kozaki, H. Umemoto, M. Sano, and T. Mukai, "Violet InGaN/GaN/AlGaN-based laser diodes operable at 50 degrees C with a fundamental transverse mode," *Japanese Journal of Applied Physics, Part 2 (Letters)* **38**, pp. L226-9, 1999.
6. D. Bour, "Nitride Lasers," Conf. Lasers and Electro-Optics CLEO, OSA, vol. 7; Baltimore, 1999.
7. M. P. Mack, A. Abare, M. Aizcorbe, P. Kozodoy, S. Keller, U. K. Mishra, L. Coldren, and S. DenBaars, "Characteristics of indium-gallium-nitride multiple-quantum-well blue laser diodes grown by MOCVD," *MRS Internet Journal of Nitride Semiconductor Research* **2**, 1997.
8. A. C. Abare, M. P. Mack, M. Hansen, R. K. Sink, P. Kozodoy, S. Keller, J. S. Speck, J. E. Bowers, U. K. Mishra, L. A. Coldren, and S. P. DenBaars, "Cleaved and etched facet nitride laser diodes," *IEEE Journal of Selected Topics in Quantum Electronics* **4**, pp. 505-9, 1998.
9. LASTIP Version 5.3.3, Crosslight Software, Inc., 1999.
10. M. Hansen, P. Fini, L. Zhao, A. C. Abare, L. A. Coldren, J. S. Speck, and S. P. DenBaars, "Improved Characteristics of InGaN Multi-Quantum Well Laser Diodes Grown on Laterally Epitaxially Overgrown GaN on Sapphire," *Applied Physics Letters* **76**, pp. 529-31, 2000.
11. M. P. Mack, G. D. Via, A. C. Abare, M. Hansen, P. K. Kozodoy, S. Keller, J. S. Speck, U. K. Mishra, L. A. Coldren, and S. P. DenBaars, "Improvement of GaN-based laser diode facets by FIB polishing," *Electronics Letters* **34**, pp. 1315-16, 1998.
12. A. C. Abare, M. P. Mack, M. Hansen, J. S. Speck, L. A. Coldren, S. P. DenBaars, G. A. Meyer, S. L. Lehew, and G. A. Cooper, "Measurement of gain current relations for InGaN multiple quantum wells," *Applied Physics Letters* **73**, pp. 3887-9, 1998.
13. Z.-M. Li, "Physical Models and Numerical Simulation of Modern Semiconductor Lasers," Physics and Simulation of Optoelectronic Devices V; ed. M. Osinski and W. W. Chow; SPIE, vol. 2994; pp: 698-708, San Jose, 1997.
14. S. L. Chuang and C. S. Chang, "A band-structure model of strained quantum-well wurtzite semiconductors," *Semiconductor Science and Technology* **12**, pp. 252-63, 1997.
15. G. Martin, A. Botchkarev, A. Rockett, and H. Morkoc, "Valence-band discontinuities of wurtzite GaN, AlN, and InN heterojunctions measured by X-ray photoemission spectroscopy," *Applied Physics Letters* **68**, pp. 2541-3, 1996.
16. C. Wetzel, T. Takeuchi, S. Yamaguchi, H. Katoh, H. Amano, and I. Akasaki, "Optical band gap in Ga(1-x)In(x)N ($0<x<0.2$) on GaN by photoreflection spectroscopy," *Applied Physics Letters* **73**, pp. 1994-6, 1998.
17. W. Gotz, N. M. Johnson, J. Walker, D. P. Bour, and R. A. Street, "Activation of acceptors in Mg-doped GaN grown by metalorganic chemical vapor deposition," *Applied Physics Letters* **68**, pp. 667-9, 1996.
18. J. H. Edgar (ed.), *Properties of Group III Nitrides*, IEE/INSPEC, London ,1994.
19. W. Gotz, N. M. Johnson, C. Chen, H. Liu, C. Kuo, and W. Imler, "Activation energies of Si donors in GaN," *Applied Physics Letters* **68**, pp. 3144-6, 1996.
20. K. Domen, A. Kuramata, R. Soejima, K. Horino, S. Kubota, and T. Tanahashi, "Lasing mechanism of InGaN-GaN-AlGaN MQW laser diode grown on SiC by low-pressure metal-organic vapor phase epitaxy," *IEEE Journal of Selected Topics in Quantum Electronics* **4**, pp. 490-7, 1998.
21. P. Mackowiak and W. Nakwaski, "Threshold currents of nitride vertical-cavity surface-emitting lasers with various active regions," *MRS Internet Journal of Nitride Semiconductor Research* **3**, 1998.
22. S. L. Chuang, "Optical gain of strained wurtzite GaN quantum-well lasers," *IEEE Journal of Quantum Electronics* **32**, pp. 1791-800, 1996.
23. Y. C. Yeo, T. C. Chong, and M. F. Li, "Electronic band structures and effective-mass parameters of wurtzite GaN and InN," *Journal of Applied Physics* **83**, pp. 1429-36, 1998.
24. T. Takeuchi, H. Takeuchi, S. Sota, H. Sakai, H. Amano, and I. Akasaki, "Optical properties of strained AlGaN and GaInN on GaN," *Japanese Journal of Applied Physics, Part 2 (Letters)* **36**, pp. L177-9, 1997.
25. S. Strite and H. Morkoc, "GaN, AlN, and InN: a review," *Journal of Vacuum Science & Technology B (Microelectronics Processing and Phenomena)* **10**, pp. 1237-66, 1992.
26. Y. C. Yeo, T. C. Chong, M. F. Li, and W. J. Fan, "Analysis of optical gain and threshold current density of wurtzite InGaN/GaN/AlGaN quantum well lasers," *Journal of Applied Physics* **84**, pp. 1813-19, 1998.
27. Y. C. Yeo, T. C. Chong, and M.-F. Li, "Uniaxial strain effect on the electronic and optical properties of wurtzite GaN-AlGaN quantum-well lasers," *IEEE Journal of Quantum Electronics* **34**, pp. 2224-32, 1998.
28. M. Asada, "Intraband Relaxation Effect on Optical Spectra," in *Quantum Well Lasers,*, ed. P. S. Zory, , pp. 97-130, Academic Press, San Diego,1993.
29. W. Fang and S. L. Chuang, "Theoretical prediction of GaN lasing and temperature sensitivity," *Applied Physics Letters* **67**, pp. 751-3, 1995.
30. L. H. Peng, C. W. Chuang, and L. H. Lou, "Piezoelectric effects in the optical properties of strained InGaN quantum wells," *Applied Physics Letters* **74**, pp. 795-7, 1999.

31. S.-H. Park and S.-L. Chuang, "Many-body optical gain of wurtzite GaN-based quantum-well lasers and comparison with experiment," *Applied Physics Letters* **72**, pp. 287-9, 1998.
32. W. W. Chow and S. W. Koch, "Theory of Laser Gain in Group-III Nitride Quantum Wells," in *GaN and Related Materials,*, ed. S. J. Pearton, , pp. 235-262, Gordon & Breach, New York,1999.
33. F. della Sala, A. di Carlo, P. Lugli, F. Bernardini, V. Fiorentini, R. Scholz, and J. M. Jancu, "Free-carrier screening of polarization fields in wurtzite GaN/InGaN laser structures," *Applied Physics Letters* **74**, pp. 2002-4, 1999.
34. W. W. Chow, A. F. Wright, A. Girndt, F. Jahnke, and S. W. Koch, "Microscopic theory of gain for an InGaN/AlGaN quantum well laser," *Applied Physics Letters* **71**, pp. 2608-10, 1997.
35. W. W. Chow, M. H. Crawford, A. Girndt, and S. W. Koch, "Threshold conditions for an ultraviolet wavelength GaN quantum-well laser," *IEEE Journal of Selected Topics in Quantum Electronics* **4**, pp. 514-19, 1998.
36. H. Y. Zhang, X. H. He, Y. H. Shih, M. Schurman, Z. C. Feng, and R. A. Stall, "Waveguide study and refractive indices of GaN:Mg epitaxial film," *Optics Letters* **21**, pp. 1529-31, 1996.
37. R. K. Sink, "Cleaved-Facet III-Nitride Laser Diodes," Ph.D. Thesis, Electrical and Computer Engineering, University of California at Santa Barbara, 2000.
38. D. K. Young, M. P. Mack, A. C. Abare, M. Hansen, L. A. Coldren, S. P. Denbaars, E. L. Hu, and D. D. Awschaloma, "Near-field scanning optical microscopy of indium gallium nitride multiple-quantum-well laser diodes," *Applied Physics Letters* **74**, pp. 2349-51, 1999.
39. D. Hofstetter, D. P. Bour, R. L. Thornton, and N. M. Johnson, "Excitation of a higher order transverse mode in an optically pumped In/sub 0.5/Ga/sub 0.85/N/In/sub 0.05/Ga/sub 0.95/N multiquantum well laser structure," *Applied Physics Letters* **70**, pp. 1650-2, 1997.
40. K. Domen, R. Soejima, A. Kuramata, K. Horino, S. Kubota, and T. Tanahashi, "Interwell inhomogeneity of carrier injection in InGaN/GaN/AlGaN multiquantum well lasers," *Applied Physics Letters* **73**, pp. 2775-7, 1998.
41. J. Piprek, P. Abraham, and J. E. Bowers, "Cavity length effects on internal loss and quantum efficiency of multiquantum-well lasers," *IEEE J. Sel. Top. Quantum Electron.* **5**, pp. 643-7, 1999.